ACS OMEGA

http://pubs.acs.org/journal/acsodf

Article

Effect of Refractory Tantalum Metal Filling on the Microstructure and Thermoelectric Properties of Co_4Sb_{12} Skutterudites

Vikrant Trivedi, Manjusha Battabyal,* Suresh Perumal, Avnee Chauhan, Dillip K. Satapathy,* Budaraju Srinivasa Murty, and Raghavan Gopalan

Cite This: *ACS Omega* 2021, 6, 3900−3909

Read Online

ACCESS | Metrics & More | Article Recommendations | Supporting Information

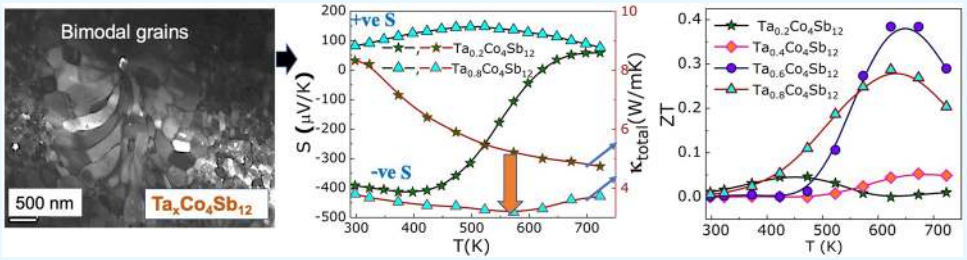

ABSTRACT: We report a systematic investigation of the microstructure and thermoelectric properties of refractory element-filled nanostructured Co_4Sb_{12} skutterudites. The refractory tantalum (Ta) metal-filled Co_4Sb_{12} samples ($Ta_xCo_4Sb_{12}$ (x = 0, 0.4, 0.6, and 0.8)) are synthesized using a solid-state synthesis route. All the samples are composed of a single skutterudite phase. Meanwhile, nanometer-sized equiaxed grains are present in the $Ta_{0.2}Co_4Sb_{12}$ and $Ta_{0.4}Co_4Sb_{12}$ samples, and bimodal distributions of equiaxed grains and elongated grains are observed in $Ta_{0.6}Co_4Sb_{12}$ and $Ta_{0.8}Co_4Sb_{12}$ samples. The dominant carrier type changes from electrons (n-type) to holes (p-type) with an increase in Ta concentration in the samples. The power factor of the $Ta_{0.6}Co_4Sb_{12}$ sample is increased to 2.12 mW/mK^2 at 623 K due to the 10-fold reduction in electrical resistivity. The lowest lattice thermal conductivity observed for $Ta_{0.6}Co_4Sb_{12}$ indicates the rattling action of Ta atoms and grain boundary scattering. Rietveld refinement of XRD data and the analysis of lattice thermal conductivity data using the Debye model confirm that Ta occupies at the voids as well as the Co site. The figure of merit (ZT) of ∼0.4 is obtained in the $Ta_{0.6}Co_4Sb_{12}$ sample, which is comparable to single metal-filled p-type skutterudites reported to date. The thermoelectric properties of the refractory Ta metal-filled skutterudites might be useful to achieve both n-type and p-type thermoelectric legs using a single filler atom and could be one of replacements of the rare earth-filled skutterudites with improved thermoelectric properties.

1. INTRODUCTION

Thermoelectric (TE) devices are useful for solid-state energy conversion technology and offer a direct conversion of heat to electricity. These devices have great potential to generate useful energy by recycling waste heat.[1,2] Many alloy systems like half-Heuslers,[1−4] skutterudites,[5−8] silicides,[9,10] tellurides,[11−14] selenides,[15] clathrates,[16] and Zintl phases[17] are being widely explored as potential materials for TE devices. The dimensionless figure of merit, $ZT = S^2T/\rho\kappa_{total}$, is a unique parameter that measures the performance of a TE material, where S, ρ, and κ_{total} are the Seebeck coefficient, electrical resistivity, and thermal conductivity, respectively, at absolute temperature T. The thermal conductivity κ_{total} arises due to the contributions from electronic thermal conductivity (κ_e) and lattice thermal conductivity (κ_l).[2] The ZT of a TE material system can be enhanced by simultaneously increasing the power factor ($PF = S^2/\rho$) and by reducing the thermal conductivity (κ_{total}). The intricate interdependence of electrical and thermal properties is a major obstacle to enhance ZT.[16] The lattice thermal conductivity, which depends mostly on the phonon vibrations, can be reduced via smart alloying,[17] nanostructure engineering,[18−20] superlattice/nanoinclusions,[21] and intrinsic manipulation of a large anharmonic lattice.[22] The power factor can be optimized by tailoring the electrical properties of the TE materials by bandgap engineering or carrier transport phenomena.[11−20] Therefore, to get the best out of a TE material system, a detailed investigation of the microstructure, electronic properties, and lattice thermal conductivity of the TE materials is required in detail.

Among the potential TE materials, Co_4Sb_{12}-based skutterudites are highly solicited for intermediate temperature range applications due to their high power factor compared to other TE materials. But the thermal conductivity of the skutterudites

Received: November 25, 2020
Accepted: January 12, 2021
Published: January 28, 2021

https://dx.doi.org/10.1021/acsomega.0c05740
ACS Omega 2021, 6, 3900−3909

is also quite high (~9 W/mK at 300 K), which can be readily reduced by following Slack's concept of phonon-glass-electron-crystal (PGEC).[23] According to Slack's concept, the scattering of heat-carrying phonons in cage-like compounds (e.g., clathrates, Zintl phases, and skutterudites) can be enhanced by the rattling of trapped heavy atoms.[17−19] The Co_4Sb_{12} skutterudites consist of a cubic structure (space group $Im\bar{3}$), with planar four-membered Sb_4 rectangle rings located at the six body-centered (bcc) positions, and two large Sb icosahedral voids are present at the remaining two bcc positions. The voids can be occupied by filler atom X (X can be an alkaline metal, alkaline-earth metal, rare-earth metal, transition metal (Ag, Au, Tl, Cd, Pb, and In), and chalcogenide (Se, Te, etc.)) to form a filled skutterudite $X_mCo_4Sb_{12}$ (m is the atomic fraction of X atom).[6−18] The positions of X, Co, and Sb atoms are at the 2a site (0, 0, 0), 8c site (1/4, 1/4, 1/4), and 24g site (0, y, z), respectively. The fillers' vibrations lead to strong scattering of phonons, resulting in a significant reduction in lattice thermal conductivity.[18,19] Single, double, and multiple atom filling approaches are being adopted in skutterudites to reduce the lattice thermal conductivity (κ_l). But there are practical issues in using the multiple fillers in terms of stability, reproducibility, ease of handling, and cost. The highly reactive nature of the alkali and alkaline-earth metals are not suitable to be filled in the skutterudite cages. Also, the low melting point of chalcogen metals are not suitable fillers for skutterudites as they show sublimation at elevated temperatures in a long thermal run.

Herein, our approach is to replace the traditional rare-earth filler atoms with cost-effective new filler atoms that will easily be processed and can be stable during repeated thermal cycles. We have adopted tantalum (Ta) as a refractory filler candidate for skutterudites and, to the authors' best knowledge, no work on Ta-filled skutterudites is reported so far in the literature. Due to the bigger size, Ta is used as a doping element in half-Huesler TE alloys to enhance the TE properties.[24,25] The basic criterion for the selection of Ta as a filler atom is that it has a covalent radius of 1.70 Å, which is smaller than the void radius (1.892 Å),[19] and hence, it can be filled in the void space easily. Further, there is also a possibility that Ta can go to the Co site and replace the Co atom from the lattice. The electronegativity of Ta (1.5) is less than that of Sb (2.1), one of the important criteria for Ta to be fitted in the skutterudite voids. It is also noteworthy that a large difference in electronegativities between the filler and the host Sb atoms is beneficial for electron transport in skutterudites.[8] Therefore, to understand the effect of refractory metal filling on the thermoelectric properties of Co_4Sb_{12} skutterudites, phase pure nanocrystalline Ta-filled Co_4Sb_{12} ($Ta_xCo_4Sb_{12}$ (x = 0.2, 0.4, 0.6, and 0.8)) samples are synthesized via ball milling and the spark plasma sintering route. The bimodal grains are observed in the samples with higher Ta concentrations (x = 0.6 and 0.8). While the Seebeck coefficients of $Ta_xCo_4Sb_{12}$ (x = 0.2 and 0.4) samples are n-type, the $Ta_{0.8}Co_4Sb_{12}$ sample is fully p-type throughout the investigated temperature region (300−723 K). There is a remarkable enhancement of TE properties in the $Ta_{0.6}Co_4Sb_{12}$ sample due to the simultaneous reduction of electrical resistivity and lattice thermal conductivity.

2. EXPERIMENTAL PROCEDURE

2.1. Sample Preparation. The polycrystalline $Ta_xCo_4Sb_{12}$ (where x = 0.2, 0.4, 0.6, and 0.8) samples were prepared by ball milling and the spark plasma sintering route as discussed elsewhere.[26] The powders of the constituent elements Co (99.8%), Sb (99.8% purity), and Ta (99.9%) were ball-milled in a Retsch Ball Mill for 10 h in a WC-Co grinding medium under an inert gas atmosphere. The milled powders were sintered at 873 K and 50 MPa uniaxial pressure using a Spark Plasma Sintering (SPS) unit (M/S Dr. Sinter, Model SPS-625, SPS Syntex Inc., Japan) to make cylindrical pellets having a diameter of 15 mm and a thickness of 4 mm. Two pellets were compacted from each batch of ball-milled powders for the thermoelectric characterizations.

While the Rigaku X-ray diffractometer was utilized for the structural characterization of the SPS samples, in-depth microstructures were investigated using a ZEISS Merlin scanning electron microscope and transmission electron microscope (TECNAI T20). The transmission electron microscopy (TEM) specimen is prepared by cutting 3 mm circular discs from the SPS pellets, followed by polishing and dimple grinding using a dimple grinder M/S Gatan Dimple grinder. Finally, the dimpled specimen is ion-milled (PIPS, M/S Gatan Inc., USA) to get the electron transparent sample for TEM investigations. X-ray photoelectron spectroscopy (XPS) studies were performed with a Thermo Fisher ESCALAB 250Xi+ (USA) using 300 W Al Kα radiation at a base pressure of ~8.9×10^{-10} mbar. The binding energies were referenced to the C 1s line at 284.6 eV from adventitious carbon.

The simultaneous measurements of temperature-dependent Seebeck coefficient and electrical resistivity were performed in the temperature range from 300 to 723 K by the ZEM-3M8/L system (M/S ULVAC-RIKO, Japan). A NETZSCH laser-flash apparatus was used to measure the thermal diffusivity of the samples in the temperature range of 300−773 K. To maximize the full absorption on the top surface and highest emissivity from the bottom side of the samples, a thin layer of graphite coating was applied on the samples. The thermal conductivity (κ) is determined using the equation $\kappa = D \times C_P \times d$, where D, C_P, and d are respectively the thermal diffusivity, specific heat, and bulk density of the sample. The uncertainty in each measurement is less than 5%. The bulk densities of the obtained SPS pellets were measured using the Archimedes principle in an ethanol medium.

3. RESULTS AND DISCUSSION

3.1. XRD, SEM, and TEM Investigations. Figure 1 shows XRD patterns from $Ta_xCo_4Sb_{12}$ (x = 0, 0.2, 0.4, 0.6, and 0.8) SPS pellets. It is found that all the samples are having a single-phase skutterudite structure of $Im\bar{3}$ symmetry. The inset in Figure 1a shows the gradual shifting of the Bragg peak at 2θ = 31.2°, the most intense peak from the (013) plane of the $CoSb_3$ skutterudite phase, toward the left with an increase in

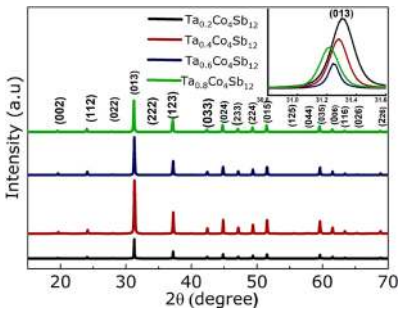

Figure 1. X-ray diffraction pattern of SPS pellets; the inset shows peak shifting of the (013) plane

https://dx.doi.org/10.1021/acsomega.0c05740
ACS Omega 2021, 6, 3900−3909

Ta concentration. It is because the lattice parameter of the $CoSb_3$ lattice increases with an increase in Ta concentration. The increase in the lattice parameter with an increase in Ta concentration might be due to either (a) Ta occupancy in the voids and/or (b) Ta replacing the Co of the skutterudite lattice. Considering the void occupancy by the Ta atom, the Rietveld refinement patterns are depicted in Figure 2a. For more details, see Figure S1, Supporting Information. It manifests that Ta is entering into the filling site 2a (0, 0, 0), having a higher isotropic atomic displacement parameter. Ta-filling fraction values and other refinement results are shown in Table S1, Supporting Information. Figure 2b and Figure S2, Supporting Information, show the Rietveld refinement of XRD data considering the occupancy of Ta at the Co (1/4, 1/4, 1/4) site. In both types of XRD data refinement, no impurity phase is found. The previous report on filled skutterudites shows the simultaneous filling and Co substitution by the filler atoms, which would lead to an increase in lattice parameter.[27,28] The crystallite size calculated from the XRD data using the full-width half maxima (FWHM) of the most intense peak from the (013) plane shows the nanocrystalline nature of the samples (Table 1). The nanocrystalline nature of skutterudites processed by the powder metallurgy route is also reported earlier.[7,8,19]

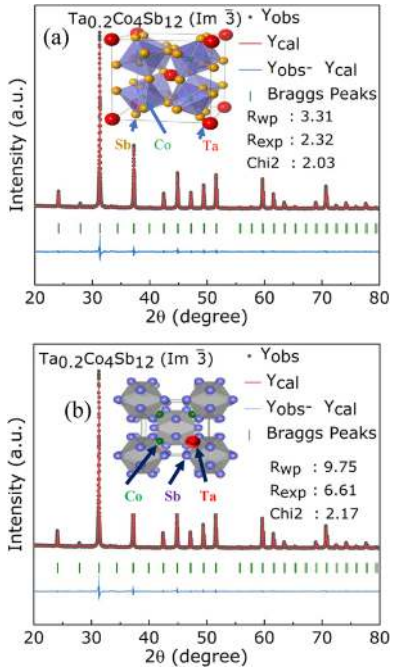

Figure 2. Rietveld fitting of the $Ta_{0.2}Co_4Sb_{12}$ sample using the assumption that (a) Ta will occupy the void 2a site (0, 0, 0) and (b) Ta substitutes the Co site 8c (1/4, 1/4, 1/4). Insets in (a) and (b) show the corresponding unit cell of the crystal structure of Ta-filled Co_4Sb_{12} in which Co, Sb, and Ta are represented by small-, medium-, and large-sized spheres, respectively. Visualized with VESTA, where the Ta atom, arrows, and the name of the elements are added.[54]

The scanning electron microscopy (SEM) micrographs of the freshly prepared fractured surfaces of the samples at low and higher magnifications are respectively illustrated in the left and right sides of Figure 3 and Figure S3. From Figure 3 and Figure S3, it is observed that nanometer-sized equiaxed grains (~85 nm) are present in all the samples. In the case of $Ta_{0.6}Co_4Sb_{12}$ and $Ta_{0.8}Co_4Sb_{12}$ samples, the bimodal distribution of grains having elongated banana-like dendrite grains is distinctly visible (marked as dotted circles in Figure 3). This type of grain growth is also reported in our earlier work,[19] where Ni is used as a dopant at the Co site of Dy-filled Co_4Sb_{12}. Hence, it can be predicted that dendritic grain growth might happen during the sintering of the sample preparation stage. No grain texturing is observed in any samples. With a bimodal distribution of grains, we have dissimilar grain boundaries present in $Ta_{0.6}Co_4Sb_{12}$ and $Ta_{0.8}Co_4Sb_{12}$ samples compared to $Ta_{0.2}Co_4Sb_{12}$ and $Ta_{0.4}Co_4Sb_{12}$ samples. The divergent grain boundaries might lead to phonon scattering at a large scale.[29] As observed in Figure 3, the grains are highly close-packed. This indicates the high bulk volume mass density of the processed samples. The density evaluated using the Archimedes principle shows ~7.65 g/cc in all samples, which is 98% of theoretical density (Table 1). An EDS study has been performed in the fractured surface of the samples over a large area (5 μm × 5 μm) to know the actual composition of Ta, Co, and Sb and is tabulated in Table 1. It is observed that although the exact composition slightly differs from the nominal composition, the skutterudite phase remains intact in all the samples as observed from the XRD data (Figure 1).

To further investigate the grain distribution in the samples, TEM has been carried out on the $Ta_{0.4}Co_4Sb_{12}$ and $Ta_{0.6}Co_4Sb_{12}$ samples. Figure 4 and Figure S4, Supporting Information, show the typical bright-field TEM images and corresponding selected area electron diffraction (SAED) pattern from both the samples. The $Ta_{0.4}Co_4Sb_{12}$ sample shows well-angular grains with an average size of ~85 nm. These grain sizes (<100 nm) are matched with previously synthesized $CoSb_3$ using the solid-state synthesis route.[19] The SAED pattern obtained from $Ta_{0.4}Co_4Sb_{12}$ confirms the $CoSb_3$ skutterudite phase (Figure 4b). Figure 4c,d shows the bright-

Table 1. Values of Some Physical Properties of Investigated Samples

sample	$Ta_{0.2}Co_4Sb_{12}$	$Ta_{0.4}Co_4Sb_{12}$	$Ta_{0.6}Co_4Sb_{12}$	$Ta_{0.8}Co_4Sb_{12}$
nominal composition	1.23:24.69:74.07	2.44:24.40:73.16	3.61:24.09:72.28	4.76:23.80:71.43
actual composition	1.25:24.73:74.01	2.56:26.23:71.01	3.78:24.23:71.99	4.85:24.05:71.10
crystallite size (nm)	47.18	59.2	48.3	58.5
lattice parameter (Å)	9.0207	9.031	9.0432	9.0516
grain size (nm)	85	85	75/185	80/210
density (g/cc)	7.62	7.75	7.74	7.73
ρ at 300 K (10^{-5} Ω·m)	46.7	34.6	11.6	9.6
κ_l at 300 K (W/m·K)	8.30	6.38	5.78	5.60
S at 300 K (μV/K)	−391	−33	−41	82
n (10^{20} cm^{-3}) at 300 K	0.19	2.97	3.7	5.1

https://dx.doi.org/10.1021/acsomega.0c05740
ACS Omega 2021, 6, 3900−3909

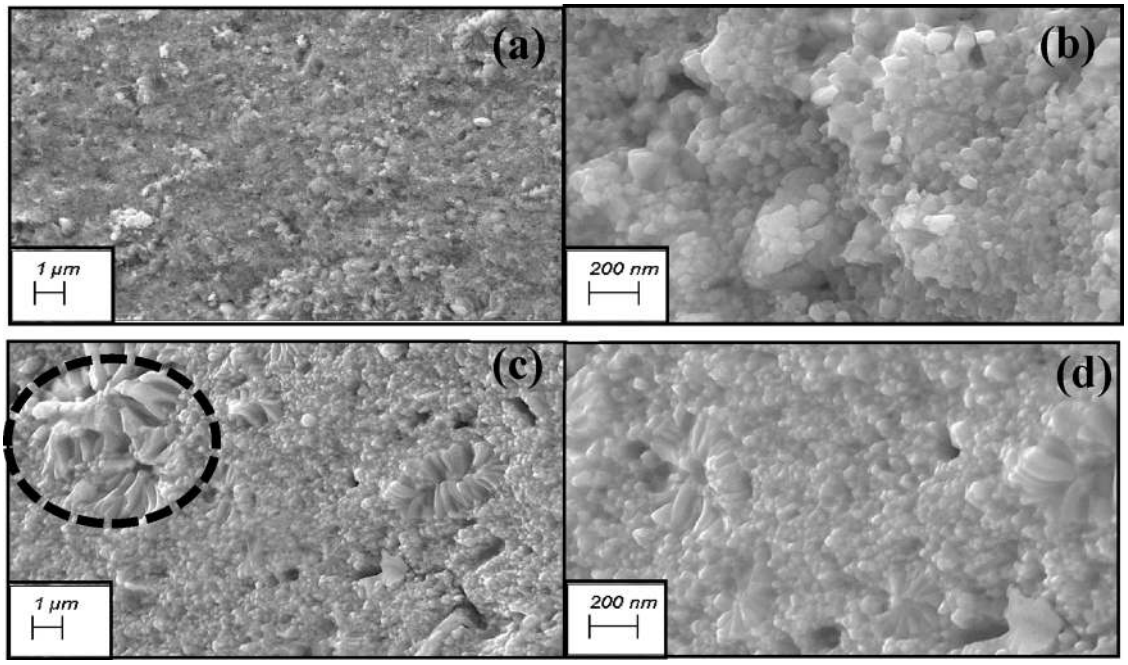

Figure 3. SEM images of the fracture surface of (a, b) $Ta_{0.2}Co_4Sb_{12}$ and (c, d) $Ta_{0.8}Co_4Sb_{12}$. Right-side images are higher-magnification images of (a) and (c). The dashed circle shows the larger grains present in the sample.

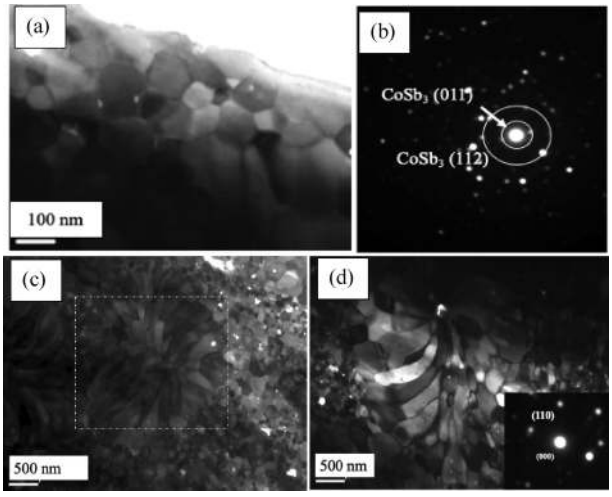

Figure 4. (a) Typical TEM bright-field image of the $Ta_{0.4}Co_4Sb_{12}$ sample showing the distribution of grains, (b) SAED pattern from the $Ta_{0.4}Co_4Sb_{12}$ sample, and (c, d) typical TEM bright-field image of $Ta_{0.6}Co_4Sb_{12}$ showing the bimodal distribution of grains; the inset in (d) shows the diffraction. We can see growth of larger grains at the expense of small grains from (c) and (d); the dotted square in (c) shows clear evidence of dendritic grain growth.

field TEM images of the $Ta_{0.6}Co_4Sb_{12}$ sample, confirming the bimodal distribution of grains. It is also observed that large dendritic grains with a size of ∼200 nm are present along with the equiaxed small grains (∼85 nm). Figure 4b and inset of Figure 4d show the SAED pattern from small and big grains, respectively. All the SAED patterns correspond to the cubic $CoSb_3$ structure. There is no secondary phase or any precipitates observed in any samples. Hence, it can be concluded that the obtained bimodal grains are having a skutterudite phase and may arise during the sintering process as explained in the literature.[19] It is known that both sintering temperature and milling conditions are crucial for inducing abnormal grain growth. The milling conditions determine the size of the starting powders, while the sintering temperature affects grain growth. When the grain size is fine and uniform, only continuous grain growth occurs at low sintering temperatures. As the sintering temperature is high enough, some grains stop growing, while the others experience rapid growth, leading to the bimodal grains.

3.2. XPS Investigations. To understand the binding states of Sb and Ta, we have carried out X-ray photoelectron spectroscopy (XPS) measurements of the samples. Due to the measurement limitations, XPS was carried out on $Ta_{0.2}Co_4Sb_{12}$ and $Ta_{0.8}Co_4Sb_{12}$ samples and is depicted in Figure 5. Figure 5 shows the deconvolution XPS spectra from Co 2p, Sb 3d, and Ta 4f orbitals of $Ta_{0.2}Co_4Sb_{12}$ and $Ta_{0.8}Co_4Sb_{12}$ samples. The binding energy of Ta at 25.67 and 27.8 eV of $4f_{5/2}$ and $4f_{7/2}$ corresponds to Ta^{4+} and Ta^{5+}, respectively.[27] The binding energy of Ta peaks is shifting ∼0.2 eV higher in $Ta_{0.8}Co_4Sb_{12}$ samples (Tables S3−S5). It means the less electron cloud on the Ta site for the $Ta_{0.8}Co_4Sb_{12}$ sample compared to the $Ta_{0.2}Co_4Sb_{12}$ sample. The binding energies of Co 2p are almost the same in both the samples and hence, only Co^{3+} is present in the samples.[28] But the interesting part is that Sb $3d_{5/2}$ and $3d_{3/2}$ peaks are shifted toward lower binding energies with an increase in Ta concentration. In the case of the filled skutterudite, the $[Sb_4]^{-4}$ ring acts as an acceptor, and the bonding in the Sb−Sb ring changes when a filler atom is added. There are four peaks of Sb in the case of the $Ta_{0.2}Co_4Sb_{12}$ sample, which are at 528.27, 530.59, 532.08, and 540.05 eV. The XPS peaks at 528.27 and 530.59 eV respectively correspond to the short $\beta\beta\sigma$ Sb−Sb bond and long $\beta\beta\sigma$ Sb−Sb bond of the $[Sb_4]^{4-}$ planar ring.[28] These two bonds are shifted toward lower binding energy, i.e., 528.09 and 530.57 eV, for the $Ta_{0.8}Co_4Sb_{12}$ sample. The shifting of the XPS peaks toward lower binding energy means the more electron cloud on the $[Sb_4]^{4-}$ ring with an increase in Ta concentration. The chemical shift can be explained in terms of the difference in electronegativities of Ta (1.5) and Sb (2.05).

https://dx.doi.org/10.1021/acsomega.0c05740
ACS Omega 2021, 6, 3900−3909

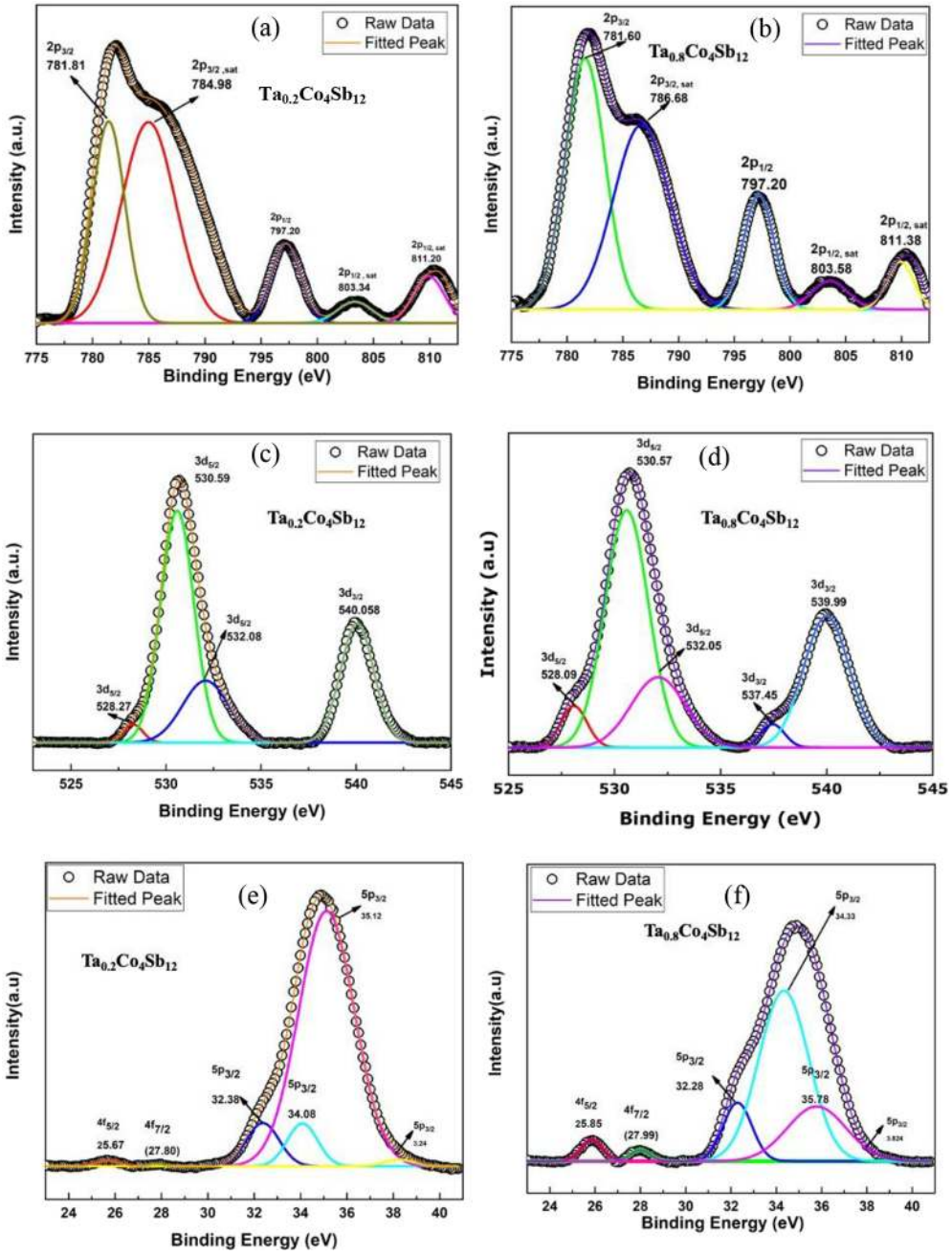

Figure 5. X-ray photoelectron spectra of (a, b) Co, (c, d) Sb, and (e, f) Ta for $Ta_{0.2}Co_4Sb_{12}$ and $Ta_{0.8}Co_4Sb_{12}$ samples.

Hence, the Ta filler in the Sb icosahedron could bring out an electron transition from Ta to Sb and result in a small enhancement in the densities of charge cloud at the $[Sb_4]^{4-}$ ring. As a result, the system tends to be a dominant positive charge carrier with an increase in Ta concentration.

3.3. Electrical Resistivity. Next, we report the variation of electrical resistivity (ρ) of $Ta_xCo_4Sb_{12}$ (x = 0.2, 0.4, 0.6, and 0.8) samples with temperature (T) in the range of 300 to 723 K and is depicted in Figure 6a. It shows the narrow bandgap semiconducting behavior of $Ta_xCo_4Sb_{12}$ samples; i.e., ρ of $Ta_xCo_4Sb_{12}$ samples decreases rapidly with an increase in temperature until 600 K and then subsequently remains constant. This counters the previously reported work on filled skutterudites where ρ increases with an increase in filler atom concentration due to the lowering of electron mobilities.[18] But it is reported that indium (In)-filled Co_4Sb_{12} shows a decrease in ρ due to the increase in electrons at the Fermi level when the In concentration increases.[28] A decrease in the ρ value with an increase in Ta concentration can be related to the increase in carrier concentration. The Ta-filled skutterudite has much lower ρ compared to the unfilled skutterudite reported earlier (ρ values at 300 K of $Ta_{0.2}Co_4Sb_{12}$ and Co_4Sb_{12} are 46.7 × 10^{-5} and 5 × 10^{-3} Ω·m, respectively).[26]

The bandgaps of the samples at different temperature regions are calculated by fitting the $\rho-T$ data using the Arrhenius equation $\rho(T) = \rho_0 \exp\left(\frac{E_g}{2k_BT}\right)$, where ρ_0 is the pre-exponential constant in the fitted region, E_g is the bandgap/energy gap, and k_B is the Boltzmann constant.[7] The bandgap of the samples decreases with an increase in Ta concentration as

https://dx.doi.org/10.1021/acsomega.0c05740
ACS Omega 2021, 6, 3900−3909

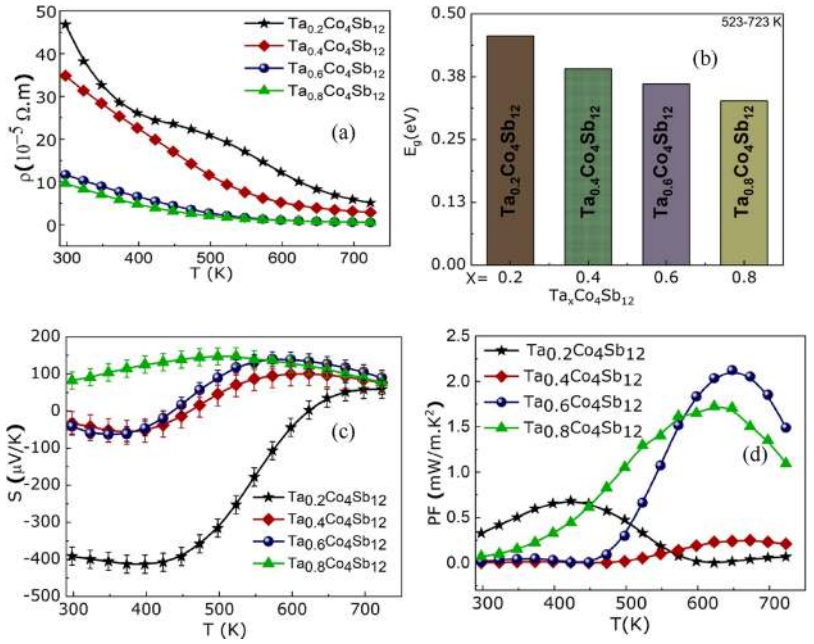

Figure 6. (a) Temperature dependence of electrical resistivity, (b) bandgap dependency of filling fraction over 298−423 K and 523−723 K, (c) Seebeck coefficient, and (d) power factor of $Ta_xCo_4Sb_{12}$.

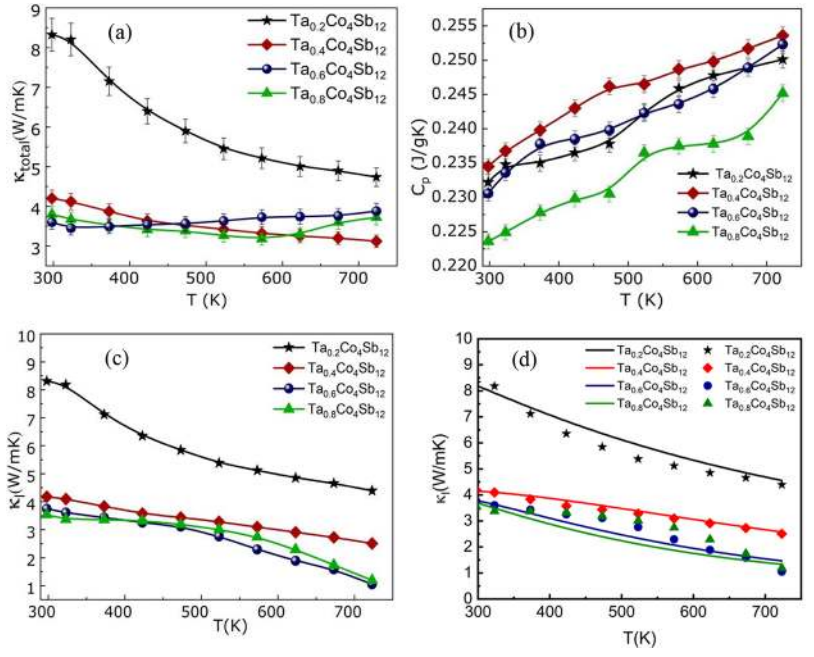

Figure 7. Temperature variation of (a) total thermal conductivity, (b) specific heat, and (c) lattice thermal of $Ta_xCo_4Sb_{12}$ from 300 to 723 K. (d) Fitting of lattice thermal conductivity using the Debye model. Points show the measured lattice thermal conductivity values and the corresponding line shows the Debye model fitting of lattice thermal conductivity considering various phonon scattering rates.

depicted in Figure 6b. In the case of $Ta_{0.2}Co_4Sb_{12}$, E_g is 0.46 eV and it is reduced to 0.33 in the case of the $Ta_{0.8}Co_4Sb_{12}$ sample. The decrease in bandgap with an increase in Ta concentration at the 523−723 K range (Figure 6b) is due to the presence of more charge carriers at the Fermi level.[29,30]

3.4. Seebeck Coefficient and Power Factor. Further, the temperature variation of Seebeck coefficients (S) of $Ta_{0.2}Co_4Sb_{12}$, $Ta_{0.4}Co_4Sb_{12}$, $Ta_{0.6}Co_4Sb_{12}$, and $Ta_{0.8}Co_4Sb_{12}$ samples have been measured from 300 to 723 K and are plotted in Figure 6c. At 300 K, the S values of $Ta_{0.2}Co_4Sb_{12}$, $Ta_{0.4}Co_4Sb_{12}$, and $Ta_{0.6}Co_4Sb_{12}$ are negative, indicating the conduction by n-type charge carriers, while $Ta_{0.8}Co_4Sb_{12}$ has a positive S value, confirming the dominance of p-type charge carriers from 300 to 723 K. The sign change of the Seebeck coefficient from n-type to p-type with an increase in Ta concentration can be related to the more charge cloud at the $[Sb_4]^{-4}$ ring as observed from XPS observation (Figure 5). The highest value of n-type S at 300 K is observed in the case of $Ta_{0.2}Co_4Sb_{12}$ (∼−391 μV/K) and the S value decreases with an increase in Ta concentration. As the temperature is increased beyond 400 K, the value of S is found to be continuously decreased. It might be due to the existence of

https://dx.doi.org/10.1021/acsomega.0c05740
ACS Omega 2021, 6, 3900−3909

Table 2. Values of Some Phonon Scattering Parameters Evaluated by Fitting the Debye Model to the Experimental Lattice Thermal Conductivity Data

phonon scattering rates	$Ta_{0.2}Co_4Sb_{12}$	$Ta_{0.4}Co_4Sb_{12}$	$Ta_{0.6}Co_4Sb_{12}$	$Ta_{0.8}Co_4Sb_{12}$
τ_{reso}^{-1} (10^{12} S^{-1}) (300 K/773 K)	0.32/1.23	1.8/2.6	3.5/3.8	4.52/4.9
τ_{p}^{-1} (10^{12} S^{-1}) (300 K/773 K)	0.2/0.58	0.32/0.75	0.51/0.82	0.73/1.12

bipolar effect and depletion of extrinsic charge carriers at higher temperatures as observed in other skutterudites.[31,32] Proper doping at the Co or Sb site will reduce the bipolar effect in $Ta_{0.2}Co_4Sb_{12}$ and $Ta_{0.4}Co_4Sb_{12}$ samples to make them completely n-type skutterudites.[33] The positive S value of higher Ta filled sample is comparable with the earlier reported skutterudites filled with Ba/Ca/Ce/Eu/La/Nd.[6] The carrier concentration (n) is calculated by fitting Mott's equation ($S = \frac{8\pi^2 k_B^2 T}{3eh^2} m^{*3/2}$, where k_B, h, and m^* are the Boltzmann constant, Planck's constant, and effective mass, respectively)[34] to the $S-T$ data and is tabulated in Table 1. The value of m^* is calculated using a simple parabolic model and is found to vary from 0.26 m_e to 0.58 m_e with an increase in Ta concentration from 0.2 to 0.8 in the Co_4Sb_{12} lattice. It reveals that n increases drastically with an increase in filling fraction and, consequently, S decreases. Although m^* increases with an increase in Ta concentration, the subsequent increase in n reduces the Seebeck coefficient when the Ta concentration increases. From the temperature-dependent Seebeck coefficient data of $Ta_xCo_4Sb_{12}$, it can be concluded that by proper doping at the Co/Sb site, lower concentration Ta-filled skutterudites ($Ta_{0.2}Co_4Sb_{12}$ and $Ta_{0.4}Co_4Sb_{12}$) can be used as a n-type skutterudite, while higher fraction Ta-filled samples ($Ta_{0.6}Co_4Sb_{12}$ and $Ta_{0.8}Co_4Sb_{12}$) can be used as a p-type skutterudite. The above observations reveal that single refractory Ta metal can help achieve both n-type and p-type skutterudites with improved thermoelectric performance.

The power factor (PF) is a great tool to investigate the TE performance of a material. The power factor (PF) was mathematically calculated from the measured Seebeck coefficient (S) and the electrical resistivity (ρ) as the formula given: $PF = S^2/\rho$.[19] As shown in Figure 6d, the PF of samples has an irregular trend due to the irregular trend of S. The highest value of PF achieved in p-type $Ta_{0.6}Co_4Sb_{12}$ is ~2.12 mW/mK^2 at 623 K, which is reasonably high.[26] This happens because of the higher Seebeck coefficient and lower electrical resistivity as compared to pristine compounds. N-type $Ta_{0.2}Co_4Sb_{12}$ has PF ≈ 0.7 mW/mK^2, which can be enhanced by proper doping at the Co site.

3.5. Thermal Conductivity. At this juncture, it is important to investigate the thermal conductivity to understand the efficiency of the samples. Figure 7a shows the total thermal conductivity (κ_{total}) as a function of temperature for $Ta_{0.2}Co_4Sb_{12}$, $Ta_{0.4}Co_4Sb_{12}$, $Ta_{0.6}Co_4Sb_{12}$, and $Ta_{0.8}Co_4Sb_{12}$ samples between 300 and 723 K. All the samples show a decreasing trend of κ_{total} with an increase in T. The value of κ_{total} is less than that of pure unfilled Co_4Sb_{12} processed using the powder metallurgy route.[7] At 300 K, κ_{total} values of $Ta_{0.2}Co_4Sb_{12}$, $Ta_{0.4}Co_4Sb_{12}$, $Ta_{0.6}Co_4Sb_{12}$, and $Ta_{0.8}Co_4Sb_{12}$ are 8.3, 4.1, 3.8, and 3.7 W/mK, respectively. The specific heat (C_p) (Figure 7b) used for κ_{total} calculations in our study (0.22–0.25 $J\cdot g^{-1}\cdot K^{-1}$) is higher than that of other previously reported filled Co_4Sb_{12} (~0.23 $J\cdot g^{-1}\cdot K^{-1}$).[32] Wiedemann–Franz law (WFL), $\kappa_e = LT/\rho$, is used to separate the electronic and lattice thermal conductivity values, where L is the Lorentz number. For a degenerate thermoelectric semiconductor, L can be approximated as $L = 1.5 + \exp\left(\frac{-|S|}{116}\right)$, where L is in 10^{-8} $W\Omega K^{-2}$ and S is in $\mu V/K$.[35] The value of L is found to be in between 1.55 and 2.1 × 10^{-8} $W\Omega K^{-2}$ in the temperature range of 300 to 723 K. Following the value of L, the electronic contribution (κ_e) is calculated from the measured electrical resistivity and illustrated in Figure S5. The electronic part (κ_e) progressively increases as the Ta content in $Ta_xCo_4Sb_{12}$ increases. Due to the higher resistivity of $Ta_{0.2}Co_4Sb_{12}$ and $Ta_{0.4}Co_4Sb_{12}$ samples, κ_e is only ~7 and 19% of the total thermal conductivity at 723 K, respectively. On the other hand, κ_e values at 723 K of $Ta_{0.6}Co_4Sb_{12}$ and $Ta_{0.8}Co_4Sb_{12}$ samples contribute ~72 and ~70%, respectively, to κ_{total}. The lattice contribution of thermal conductivity (κ_l) is evaluated by subtracting κ_e from κ_{total} and plotted in Figure 7c. Figure S6 shows the juxtaposition between κ_{total}, κ_e, and κ_l at 300 K for $Ta_xCo_4Sb_{12}$ samples. This confirms that heat transport in skutterudites is mainly dominated by both electrons and phonons. The values of κ_l at 723 K are 4.38, 2.50, 1.05, and 1.19 W/mK for $Ta_{0.2}Co_4Sb_{12}$, $Ta_{0.4}Co_4Sb_{12}$, $Ta_{0.6}Co_4Sb_{12}$, and $Ta_{0.8}Co_4Sb_{12}$, respectively, which are ~93, 80, 28, and ~30% of the total thermal conductivity, respectively. It is observed that the κ_l value of the samples decreases with increasing Ta concentration from x = 0.2 to x = 0.6 and remains almost constant for x = 0.8. The possible reason for the lattice thermal conductivity saturation after $Ta_{0.6}Co_4Sb_{12}$ might be the maximum attainable rattling effect due to higher rattler concentration as observed earlier.[36−39] Almost a 50% decrease in total thermal conductivity is found in all the samples from 300 to 723 K. This decrease could be the combined effect of the vibrations of the guest filler, the phonon scattered by the grain boundaries or interfaces, structural point-defect scattering, and the bimodal distribution of grains acting as phonon filters.[19,36−39] The thermal conductivity of the processed samples is lower than single alkaline- and alkaline earth metal-filled systems but are found to be greater than some of the rare-earth metal-filled Co_4Sb_{12}.[19,38,39] It can be further reduced by creating more point defects as illustrated in our previous work on Ni-doped Dy-filled $CoSb_3$.[19]

The reduction in lattice thermal conductivity (κ_l) with an increase in Ta concentration is explained using the Debye model.[40,41] According to the Debye theory, κ_l can be written as

$$\kappa_l = \frac{k_B}{2\pi^2 v_S}\left(\frac{k_B T}{\hbar}\right)^3 \int_0^{\theta_D/T} \frac{x^4 e^x}{\tau^{-1}(e^x - 1)^2} dx \quad (1)$$

where $x = \frac{\hbar\omega}{k_B T}$, B is the Boltzmann constant, and D is the Debye temperature, which is evaluated from the Debye frequency ω_D as $\hbar\omega_D = k_B\theta_D$ and $\omega_D = \left(\frac{6\Pi^2}{V}\right)^{1/3} v_S$.[7] The volume V of the skutterudite lattice is calculated using the obtained lattice parameter (Table 2) and increases with an increase in Ta concentration. The previously reported sound velocity v_S is considered in our calculations.[50] The total

https://dx.doi.org/10.1021/acsomega.0c05740
ACS Omega 2021, 6, 3900−3909

phonon scattering rate τ^{-1} depends on the combined effect of grain boundary scattering (τ_b^{-1}), point defects (τ_p^{-1}), resonant scattering (τ_{reso}^{-1}), and phonon−phonon Umklapp scattering (τ_U^{-1}). The various phonon scattering rates in the case of Ta-filled Co_4Sb_{12} are noted as[8,51,52] $\tau_b^{-1} = v_S/d$, $\tau_p^{-1} = \frac{Vx^4K_B^4}{4\Pi\hbar^4v_S^3}T^4\left(\sum f_i\left(1-\frac{m_i}{m}\right)^2 + \sum f_i\left(1-\frac{r_i}{r(1+\alpha(T-300))}\right)^2\right)$, $\tau_U^{-1} = \frac{2\gamma^2K_B^3V^{1/3}x^2}{(6\Pi^2)^{1/3}\hbar^2v_S^3M}T^3$, and $\tau_{reso}^{-1} = \frac{CK_B^2x^2}{\hbar^2\left(\Omega^2-\frac{K_B^2x^2}{\hbar^2}T^2\right)^2}T^2$, where $x = \frac{\hbar\omega}{k_BT}$, m represents the mass of the filler Ta atom and the Co_4Sb_{12} lattice, r is the interatomic distance, f_i indicates the number ratio of the Ta atoms to the Co_4Sb_{12} lattice, Ω is related to the resonant phonon frequency,[8] and γ is the anharmonic Grüneisen parameter. The abovementioned phonon scattering rates were evaluated to fit the κ_l vs T data. It is observed that the evaluated phonon scattering rates could explain the measured lattice thermal conductivity quite well. Figure 7d illustrates the fitting of κ_l with the Debye model and the corresponding phonon scattering parameters are given in Table 2. It can be observed from Table 2 that resonance phonon scattering and point-defect scattering increase with an increase in Ta concentration. Hence, it might be confirmed that Ta is entering into the voids, giving rise to enhancement in resonance phonon scatterings. The resonant phonon scattering rate is associated with the coherent relative motions of the Co_4Sb_{12} lattice and Ta atom.[42−47] But Ta is also occupying at the Co site to some extent due to which point-defect scattering increases marginally with an increase in Ta concentration. In our calculations, the boundary phonon scattering rate is negligible ($\tau_b^{-1} = v_S/d \approx 10^{10}$ S^{-1}). Figure S7 shows a comparison of the lattice thermal conductivity at 300 K of the studied samples with the reported filled skutterudites. It shows that the refractory Ta metal is more effective in reducing the lattice thermal conductivity of the Co_4Sb_{12} skutterudites.

3.6. Figure of Merit. A high PF incorporated with reduced thermal conductivity results in the highest dimensionless figure of merit (ZT = 0.39 ± 0.04 at 623 K) in $Ta_{0.6}Co_4Sb_{12}$. Figure 8a depicts the thermoelectric figure of merit ZT ($=S^2T/\rho\kappa_{total}$) of the investigated samples from 300 to 723 K. Except for the $Ta_{0.2}Co_4Sb_{12}$ sample, ZT increases with an increase in temperature from 300 to 773 K. The value of ZT (0.39 ± 0.04) is low compared to many rare earth-filled skutterudites, but it is more than that of alkaline, alkaline earth, and other rare earth metals with single element-filled skutterudites fabricated using the solid-state reaction.[42−47] The TE properties of the Ta-filled skutterudites might be useful to achieve both n-type and p-type thermoelectric systems using the same filler atom. For n-type, $Ta_{0.2}Co_4Sb_{12}$ is found to be the best material, which can be improved by doping at the Co site.[38−40] Similarly, with composition $x = 0.8$, we can get the best p-type with the incorporation of the Fe/Co ratio. Since Ta is smaller in size, another filler atom can be incorporated to reduce the lattice thermal conductivity and enhance the ZT of the skutterudites (atomic radius of Ta is 220 pm and covalent radius of ∼138 pm). Figure 8b exemplifies the ZT value at 623 K of the $Ta_{0.2}Co_4Sb_{12}$ sample with the reported p-type single element-filled Co_4Sb_{12} skutterudites for better comparison.[48−50] Compared to the reported work, refractory Ta metal-filled Co_4Sb_{12} shows improved thermoelectric properties

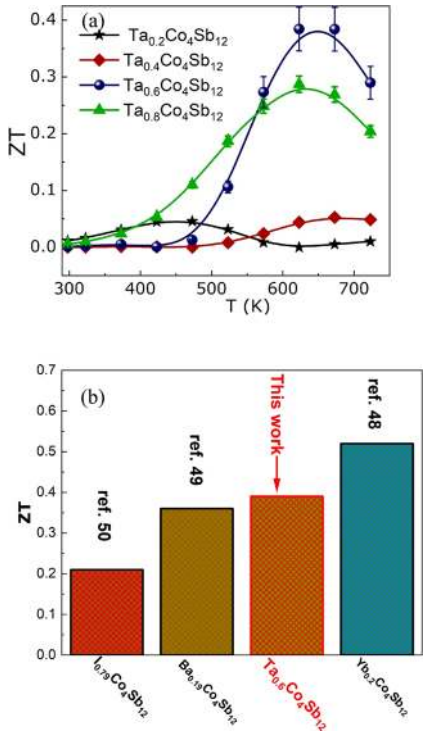

Figure 8. (a) Figures of merit of $Ta_xCo_4Sb_{12}$ samples with error bars. (b) Illustration of the comparison of ZT values of the single element-filled p-type skutterudites reported to date.[48−50]

at 623 K, although the value is a bit lower than the Yb-filled $CoSb_3$. Several other papers reported a higher ZT in Yb-filled Co_4Sb_{12} skutterudites,[51−53] but all are for n-type skutterudites and are therefore excluded from Figure 8b. The higher ZT is observed in the samples having a doping element at the Co or Sb site (Figure 8b). Hence, our investigations confirm that the cost-effective refractory metal Ta can replace the expensive rare-earth fillers in Co_4Sb_{12} skutterudites with enhancing thermoelectric performance.

4. CONCLUSIONS

In summary, the first-ever investigations of thermoelectric properties of refractory element-filled nanostructured Co_4Sb_{12} skutterudites are reported. Single-phase nanostructured Ta-filled skutterudites could be synthesized using ball milling and the spark plasma sintering route. Bimodal distribution of grains (85 and 210 nm) is observed in $Ta_{0.6}Co_4Sb_{12}$ and $Ta_{0.8}Co_4Sb_{12}$ samples. With an increase in Ta filler concentration, the Seebeck coefficient changes from n-type to p-type. The highest power factor in the p-type $Ta_{0.6}Co_4Sb_{12}$ sample is enhanced to 2.12 mW/mK^2 at 623 K due to the 10-fold reduction in electrical resistivity compared to other samples. The lattice thermal conductivity of the samples decreases continuously with an increase in Ta concentration, which can be attributed to the enhancement of phonon scattering due to Ta filler-induced resonance and point-defect scattering. The figure of merit (ZT) of ∼0.39 ± 0.04 is obtained in the $Ta_{0.6}Co_4Sb_{12}$ sample, which is higher than many other single element-filled p-type Co_4Sb_{12} skutterudites. The TE properties of the refractory Ta metal-filled skutterudites might be useful to achieve both n-type and p-type thermoelectric legs using a single filler atom and hence could be one of a replacement of

https://dx.doi.org/10.1021/acsomega.0c05740
ACS Omega 2021, 6, 3900−3909

rare earth-filled skutterudites with improved thermoelectric properties.

■ ASSOCIATED CONTENT

Supporting Information

The Supporting Information is available free of charge at https://pubs.acs.org/doi/10.1021/acsomega.0c05740.

Rietveld fitting of the XRD data and the parameters table, SEM and TEM images, electronic thermal conductivity graph, lattice thermal conductivity graph, and the table containing fitting parameters of the XPS data (PDF)

■ AUTHOR INFORMATION

Corresponding Authors

Manjusha Battabyal − *Centre for Automotive Energy Materials, International Advanced Research Center for Powder Metallurgy and New Materials, Chennai 600113, India;* orcid.org/0000-0003-1191-1136; Email: manjusha.battabyal@gmail.com

Dillip K. Satapathy − *Soft Materials Laboratory, Department of Physics, Indian Institute of Technology, Chennai 6000036, India;* orcid.org/0000-0002-3083-655X; Email: dks@iitm.ac.in

Authors

Vikrant Trivedi − *Centre for Automotive Energy Materials, International Advanced Research Center for Powder Metallurgy and New Materials, Chennai 600113, India; Department of Metallurgical and Materials Engineering, Indian Institute of Technology, Chennai 6000036, India*

Suresh Perumal − *Department of Physics and Nanotechnology, SRM Institute of Science and Technology, Kancheepuram 603203, India*

Avnee Chauhan − *Soft Materials Laboratory, Department of Physics, Indian Institute of Technology, Chennai 6000036, India*

Budaraju Srinivasa Murty − *Department of Metallurgical and Materials Engineering, Indian Institute of Technology, Chennai 6000036, India; Indian Institute of Technology Hyderabad, Sangareddy 502285, India*

Raghavan Gopalan − *Centre for Automotive Energy Materials, International Advanced Research Center for Powder Metallurgy and New Materials, Chennai 600113, India;* orcid.org/0000-0003-2871-8682

Complete contact information is available at: https://pubs.acs.org/10.1021/acsomega.0c05740

Notes

The authors declare no competing financial interest.

■ ACKNOWLEDGMENTS

The authors are grateful to Director, ARCI, and Prof. G. Sundararajan, Distinguished Scientist, ARCI, for their keen interest and support in this work. V.T., M.B., and R.G. are grateful to the Department of Science and Technology, Government of India, for financial support through a research grant (no. AI/1/65/ARCI/2014). A.C. and D.K.S. acknowledge financial support from the Ministry of Human Resource and Development (MHRD), India, through the IMPacting Research INnovation and Technology (IMPRINT-I) scheme.

■ REFERENCES

(1) Twaha, S.; Zhu, J.; Yan, Y.; Li, B. A comprehensive review of thermoelectric technology: materials, applications, modelling and performance improvement. *Renew. Sustain. Energy Rev.* **2016**, *65*, 698−726.

(2) Zhang, X.; Zhao, L. D. Thermoelectric materials: energy conversion between heat and electricity. *J Materiomics* **2015**, *1*, 92−105.

(3) Karati, A.; Murty, B. S. Synthesis of nanocrystalline half-Heusler TiNiSn by mechanically activated annealing. *Mater. Lett.* **2017**, *205*, 114−117.

(4) Karati, A.; Mukherjee, S.; Mallik, R. C.; Shabadi, R.; Murty, B. S.; Varadaraju, U. V. Simultaneous increase in thermopower and electrical conductivity through Ta-doping and nanostructuring in half-Heusler TiNiSn alloys. *Materialia* **2019**, *7*, 100410.

(5) Sales, B. C.; Mandrus, D.; Williams, R. K. Filled skutterudite antimonides: a new class of thermoelectric materials. *Science* **2008**, *272*, 1325−1328.

(6) Rogl, G.; Grytsiv, A.; Rogl, P.; Peranio, N.; Bauer, E.; Zehetbauer, M.; Eibl, O. n- type skutterudites $(R,Ba,Yb)yCo_4Sb_{12}$ (R=Sr, La, Mm, DD, SrMm, SrDD) approaching ZT∼2.0. *Acta Mater.* **2014**, *63*, 30−43.

(7) Battabyal, M.; Priyadarshini, B.; Sivaprahasam, D.; Karthiselva, N. S.; Gopalan, R. The effect of Cu_2O nanoparticle dispersion on the thermoelectric properties of n-type skutterudites. *J. Phys. D: Appl. Phys.* **2015**, *48*, 455309.

(8) Battabyal, M.; Priyadarshini, B.; Pradipkanti, L.; Satapathy, D. K.; Gopalan, R. Phase stability and lattice thermal conductivity reduction in $CoSb_3$ skutterudites, doped with chalcogen atoms. *AIP Advances* **2016**, *6*, No. 075308.

(9) Basu, R.; Bhattacharya, S.; Bhatt, R.; Roy, M.; Ahmad, S.; Singh, A.; Navaneethan, M.; Hayakawa, Y.; Aswal, D. K.; Gupta, S. K. Improved thermoelectric performance of hot pressed nanostructured n-type SiGe bulk alloys. *J. Mater. Chem. A* **2014**, *2*, 6922−6930.

(10) Nolas, G. S.; Wang, D.; Beekman, M. Transport properties of polycrystalline $Mg_2Si_{1-y}Sb_y$ ($0\leq y<0.4$). *Phys. Rev. B* **2007**, *76*, 235204.

(11) Peranio, N.; Eibl, O.; Bäßler, S.; Nielsch, K.; Klobes, B.; Hermann, R. P.; Daniel, M.; Albrecht, M.; Görlitz, H.; Pacheco, V.; Bedoya-Martínez, N.; Hashibon, A.; Elsässer, C. From thermoelectric bulk to nanomaterials: Current progress for Bi_2Te_3 and $CoSb_3$. *Phys. Status Solidi A* **2016**, *213*, 739−749.

(12) Banik, A.; Vishal, B.; Perumal, S.; Datta, R.; Biswas, K. The origin of low thermal conductivity in $Sn_{1-x}Sb_xTe$: phonon scattering via layered intergrowth nanostructures. *Energy Environ. Sci.* **2016**, *9*, 2011−2019.

(13) Banik, A.; Shenoy, U. S.; Saha, S.; Waghmare, U. V.; Biswas, K. High power factor and enhanced thermoelectric performance of SnTe- $AgInTe_2$: Synergistic effect of resonance level and valence band convergence. *J. Am. Chem. Soc.* **2016**, *138*, 13068−13075.

(14) Wu, H. J.; Zhao, L.-D.; Zheng, F. S.; Wu, D.; Pei, Y. L.; Tong, X.; Kanatzidis, M. G.; He, J. Q. Broad temperature plateau for thermoelectric figure of merit ZT>2 in phase-separated $PbTe_{0.7}S_{0.3}$. *Nat. Commun.* **2014**, *5*, 4515.

(15) Bhattacharya, S.; Bohra, A.; Basu, R.; Bhatt, R.; Ahmad, S.; Meshram, K. N.; Debnath, A. K.; Singh; Sarkar, S. K.; Navneethan, M.; Hayakawa, Y.; Aswal, D. K.; Gupta, S. K. High thermoelectric performance of $(AgCrSe_2)_{0.5}(CuCrSe_2)_{0.5}$nano-composites having all-scale natural hierarchical architectures. *J. Mater. Chem. A* **2014**, *2*, 17122.

(16) Tritt, T. M. Thermoelectric Phenomena, Materials, and Applications. *Annu. Rev. Mater. Res.* **2011**, *41*, 433−448.

(17) Snyder, G. J.; Christensen, M.; Nishibori, E.; Caillat, T.; Iversen, B. B. Disordered zinc in Zn_4Sb_3 with phonon-glass and electron-crystal thermoelectric properties. *Nat. Mater.* **2004**, *3*, 458−463.

(18) Uher, C. in *Semiconductors and Semimetals*, Vol. *69*, Recent Trends in Thermoelectric Materials Research, edited by Tritt, T. M. (Academic, San Diego, 2000), pp. 139−253.

https://dx.doi.org/10.1021/acsomega.0c05740
ACS Omega 2021, 6, 3900−3909

(19) Trivedi, V.; Battabyal, M.; Balasubramanian, P.; Muralikrishna, G. M.; Jain, P. K.; Gopalan, R. Microstructure and doping effect on the enhancement of the thermoelectric properties of Ni doped Dy filled CoSb3 skutterudites. *Sustainable Energy Fuels* **2018**, *2*, 2687−2697.
(20) Biswas, K.; He, J.; Blum, I. D.; Wu, C.-I.; Hogan, T. P.; Seidman, D. N.; Dravid, V. P.; Kanatzidis, M. G. High-performance bulk thermoelectrics with all-scale hierarchical architectures. *Nature* **2012**, *489*, 414−418.
(21) Delaire, O.; Ma, J.; Marty, K.; May, A. F.; McGuire, M. A.; Du, M. H.; Singh, D. J.; Podlesnyak, A.; Ehlers, G.; Lumsden, M. D.; et al. Giant anharmonic phonon scattering in PbTe. *Nat. Mater.* **2011**, *10*, 614−619.
(22) Guin, S. N.; Biswas, K. Cation disorder and bond anharmonicity optimize the thermoelectric properties in kinetically stabilized rocksalt $AgBiS_2$ nanocrystals. *Chem. Mater.* **2013**, *25*, 3225−3231.
(23) Slack, G. A. *CRC handbook of thermoelectrics*; CRC Press: New York, 1995; pp. 407−440.
(24) Zhao, D.; Zuo, M.; Wang, Z.; Teng, X.; Geng, H. Synthesis and thermoelectric properties of tantalum-doped ZrNiSnhalf-Heusler alloys. *Funct. Mater. Lett.* **2014**, *07*, 1450032.
(25) Yu, J.; Fu, C.; Liu, Y.; Xia, K.; Aydemir, U.; Chasapis, T. C.; Snyder, G. J.; Zhao, X.; Zhu, T. Unique Role of Refractory Ta Alloying in Enhancing the Figure of Merit of NbFeSb Thermoelectric Materials. *Adv. Energy Mater.* **2018**, *8*, 1701313.
(26) Battabyal, M.; Karthiselva, N. S.; Rajesh, P.; Gopalan, R. Pressure-induced enhancement in the thermoelectric and mechanical properties of Ni-doped skutterudites during spark plasma sintering. *Mater. Innovations* **2020**, 1.
(27) Abbas, Y.; Jeon, Y. R.; Sokolov, A. S.; Kim, S.; Ku, B.; Choi, C. Compliance-Free, Digital SET and Analog RESET Synaptic Characteristics of Sub-Tantalum Oxide Based Neuromorphic Device. *Sci. Rep.* **2018**, *8*, 1228.
(28) Zhao, W.; Wei, P.; Zhang, Q.; Dong, C.; Liu, L.; Tang, X. Enhanced thermoelectric performance in barium and indium double-filled skutterudite bulk materials via orbital hybridization induced by indium filler. *J. Am. Chem. Soc.* **2009**, *131*, 3713−3720.
(29) He, T.; Chen, J.; Rosenfeld, H. D.; Subramanian, M. A. Thermoelectric properties of indium-filled skutterudites. *Chem. Mater.* **2006**, *18*, 759−762.
(30) Singh, D. J.; Pickett, W. E. skutterudite antimonides: quasilinear bands and unusual transport. *Phys. Rev. B* **1994**, *50*, 11235−11238.
(31) Caillat, T.; Borshchevsky, A.; Fleurial, J. P. Properties of single crystalline semiconducting $CoSb_3$. *J. Appl. Phys.* **1996**, *80*, 4442−4449.
(32) Kawaharada, Y.; Kurosaki, K.; Uno, M.; Yamanaka, S. Thermoelectric properties of $CoSb_3$. *J. Alloys Compd.* **2001**, *315*, 193−197.
(33) Rowe, D. M. *CRC Handbook of Thermoelectrics* (Washington DC: CRC Press), 1995 pp. 30−61.
(34) Yang, J.; Zhang, L.; Liu, Y.; Chen, C.; Li, J.; Yu, D.; He, J.; Liu, Z.; Tian, Y.; Xu, B. Investigation of skutterudite $Mg_yCo_4Sb_{12}$: High pressure synthesis and thermoelectric properties. *J. Appl. Phys.* **2013**, *113*, No. 053711.
(35) Kim, H. S.; Gibbs, Z. M.; Tang, Y.; Wang, H.; Snyder, G. J. Characterization of Lorenz number with Seebeck coefficient Measurement. *APL Mater.* **2015**, *3*, No. 041506.
(36) Dahal, T.; Jie, Q.; Joshi, G.; Chen, S.; Guo, C.; Lan, Y.; Ren, Z. Thermoelectric property enhancement in Yb-doped n-type skutterudites $Yb_xCo_4Sb_{12}$. *Acta Mater.* **2014**, *75*, 316−321.
(37) Morelli, D. T.; Meisner, G. P.; Chen, B.; Hu, S.; Uher, C. Cerium filling and doping of cobalt triantimonide. *Phys. Rev. B* **1997**, *56*, 7376−7383.
(38) Tang, X.; Zhang, Q.; Chen, L.; Goto, T.; Hirai, T. Synthesis and thermoelectric properties of p-type- and n-type-filled skutterudite $R_yM_xCo_{4-x}Sb_{12}$(R:Ce,Ba,Y; M:Fe,Ni). *J. Appl. Phys.* **2005**, *97*, No. 093712.
(39) Duan, B.; Yang, J.; Salvador, J. R.; He, Y.; Zhao, B.; Wang, S.; Wei, P.; Ohuchi, F. S.; Zhang, W.; Hermann, R. P.; Gourdon, O.; Mao, S. X.; Cheng, Y.; Wang, C.; Liu, J.; Zhai, P.; Tang, X.; Zhang, Q.; Yang, J. Electronegative Guests in $CoSb_3$. *Energy Environ. Sci.* **2016**, *9*, 2090−2098.
(40) Callaway, J. Model for Lattice Thermal Conductivity at Low Temperatures. *Phys. Rev.* **1959**, *113*, 1046−1051.
(41) Pohl, R. O. Thermal conductivity and phonon resonance scattering. *Phys. Rev. Lett.* **1962**, *8*, 481−483.
(42) Guo, L.; Xu, X.; Salvador, J. R.; Meisner, G. P. Coupled vibrational modes in multiple-filled skutterudites and the effects on lattice thermal conductivity reduction. *Appl. Phys. Lett.* **2013**, *102*, 111905.
(43) Rogl, G.; Zhang, L.; Rogl, P.; Grytsiv, A.; Falmbigl, M.; Rajs, D.; Kriegisch, M.; Müller, H.; Bauer, E.; Koppensteiner, J. Thermal Expansion of Skutterudites. *J. Appl. Phys.* **2010**, *107*, No. 043507.
(44) Feldman, J. L.; Dai, P.; Enck, T.; Sales, B. C.; Mandrus, D.; Singh, D. J. Lattice vibrations in $La(Ce)Fe_4Sb_{12}$and$CoSb_3$: Inelastic neutron scattering and theory. *Phys. Rev. B* **2006**, *73*, No. 014306.
(45) Park, K.-H.; Seo, W.-S.; Shin, D.-K.; Kim, I.-H. Thermoelectric properties of Yb-filled $CoSb_3$ skutterudites. *J. Korean Phys. Soc.* **2014**, *65*, 491−495.
(46) Park, K.-H.; Lee, S.; Seo, W.-S.; Baek, S.; Shin, D.-K.; Kim, I.-H. Thermoelectric Properties of La-filled $CoSb_3$ Skutterudites. *J. Korean Phys. Soc.* **2014**, *64*, 1004−1008.
(47) Tang, Y.; Qiu, Y.; Xi, L.; Shi, X.; Zhang, W.; Chen, L.; Tseng, S.-M.; Chen, S.-W.; Snyder, G. J. Phase diagram of In−Co−Sb system and thermoelectric properties of In-containing skutterudites. *Energy Environ. Sci.* **2014**, *7*, 812−819.
(48) Zhou, C.; Morelli, D.; Zhou, X.; Wang, G.; Uher, C. Thermoelectric properties of P-type Yb-filled skutterudite YbxFey-Co4-ySb12. *Intermetallics* **2011**, *19*, 1390−1393.
(49) Banik, A.; Biswas, K. Low-temperature soft-chemical synthesis and thermoelectric properties of barium-filled p-type skutterudite nanocrystals. *Mater. Sci. Semicond. Process.* **2014**, *27*, 593−598.
(50) Zhang, L.; Xu, B.; Li, X.; Duan, F.; Yan, X.; Tian, Y. Iodine-filled FexCo4−xSb12 polycrystals: Synthesis, structure, and thermoelectric properties. *Mater. Lett.* **2015**, *139*, 249−251.
(51) Tang, Y.; Hanus, R.; Chen, S.-W.; Snyder, G. J. Solubility design leading to high figure of merit in low-cost Ce-$CoSb_3$ skutterudites. *Nat. Commun.* **2015**, *6*, 7584.
(52) Tang, Y.; Chen, S.-W.; Snyder, G. J. Temperature dependent solubility of Yb in Yb−$CoSb_3$ skutterudite and its effect on preparation, optimization and lifetime of thermoelectrics. *J. Materiomics* **2015**, *1*, 75−84.
(53) Wang, S.; Salvador, J. R.; Yang, J.; Wei, P.; Duan, B.; Yang, J. High-Performance n-Type $Yb_xCo_4Sb_{12}$: from Partially Filled Skutterudites towards Composite Thermoelectrics NPG Asia Mater. 2016, *8*, e285, DOI: 10.1038/am.2016.77.
(54) Wee, D.; Kozinsky, B.; Marzari, N.; Fornari, M. Effects of filling in CoSb3: Local structure, band gap, and phonons from first principles. *Phys. Rev. B* **2010**, *81*, No. 045204.

https://dx.doi.org/10.1021/acsomega.0c05740
ACS Omega 2021, 6, 3900−3909